Neutron wave-packet tomography

G. Badurek,[1] P. Facchi,[3,6] Y. Hasegawa,[1] Z. Hradil,[4] S. Pascazio,[2,3] H. Rauch,[1] J. Řeháček,[4] and T. Yoneda[2,5]
[1]*Atominstitut der Österreichischen Universitäten, Stadionallee 2, A-1020 Wien, Austria*
[2]*Dipartimento di Fisica, Università di Bari, I-70126 Bari, Italy*
[3]*Istituto Nazionale di Fisica Nucleare, Sezione di Bari, I-70126 Bari, Italy*
[4]*Department of Optics, Palacký University, 17. listopadu 50, 772 00 Olomouc, Czech Republic*
[5]*School of Health Sciences, Kumamoto University, 862-0976 Kumamoto, Japan*
[6]*Dipartimento di Matematica, Università di Bari, I-70126 Bari, Italy*
(Received 22 November 2005; published 24 March 2006)

A tomographic technique is introduced in order to determine the quantum state of the center-of-mass motion of neutrons. Different reconstruction methods are compared and discussed. An experiment is proposed and numerically analyzed.

DOI: 10.1103/PhysRevA.73.032110 PACS number(s): 03.65.Wj, 03.65.Ta, 03.75.Dg, 03.75.Be

I. INTRODUCTION

In experimental physics one often faces the following question: "Given the outcomes of a particular set of measurements, which quantum state do they imply?" Such *inverse problems* may arise for instance when one sets up and calibrates laboratory sources of quantum states, or in the analysis of decoherence and other deteriorating effects of the environment, or in some special tasks in quantum-information processing, such as eavesdropping on a quantum channel in quantum cryptography.

The determination of the quantum state represents a highly nontrivial problem, whose history can be traced back to the early days of quantum mechanics, namely, to the Pauli problem [1,2]; the experimental validation had to wait until quantum optics opened a new era. The theoretical predictions of Vogel and Risken [3] were closely followed by the experimental realization of the suggested algorithm by Smithey *et al.* [4]. Since then many improvements and new techniques have been proposed: an up-to-date overview can be found in Ref. [5]. Recent progress in instrumentation has made it possible to apply these techniques to a variety of different quantum systems, such as fields in optical cavities, polarization and external degrees of freedom of photons, or motional states of atoms.

In this paper we propose an experiment for determining the quantum state of the center-of-mass motion of neutrons. In accordance with quantum theory, these massive particles can be associated with a wave function describing their motional state. Neutrons are suitable objects for many quantum-mechanical experiments due to their interaction with all four basic forces, the ease of detecting them with almost 100% efficiency, and their small coupling to the environment [6]. In marked contrast with light, neutron vacuum field and thermal background can usually be ignored. This makes it possible, for instance, to prepare superpositions of macroscopically separated quantum states—the so-called Schrödinger cat states—that would be extremely difficult to realize with other quantum systems because of their fragility with respect to decoherence. In all experiments performed so far, the existence of the Schrödinger cat states of neutrons has been indirectly demonstrated via interferometric effects, but the full evidence for the nonclassicality of these states, including the presence of the negative values of the reconstructed Wigner function, is still missing.

In the following we will first briefly review the present neutron interferometric techniques in Sec. II. An experimental setup will then be proposed in Sec. III for the complete reconstruction of the quantum state associated with the longitudinal motion of the center of mass of a neutron. Three conceptually different reconstruction methods will be discussed in Secs. IV–VI. Finally, we will demonstrate the feasibility of the proposed tomographic scheme by means of a numerical simulation in Sec. VII.

II. NEUTRON STATE TOMOGRAPHY

The set of measurements that can be done on neutrons to determine their quantum state is severely limited by the very low time resolution of the available detectors. In quantum optics, this obstacle can be overcome by coherently superposing the weak input field represented by the analytical signal $\hat{a}e^{i\omega t}$ with a strong local oscillator $ce^{i\omega t}$, which is classically described by its complex amplitude $c=|c|e^{i\phi}$. Notice that the phase ϕ of the local oscillator can be controlled in the experiment. The response of a realistic detector is then proportional to the intensity

$$I=\langle|\hat{a}e^{i\omega t}+ce^{i\omega t}|^2\rangle. \tag{1}$$

Since the local oscillator is assumed to be strong, $|c|^2 \gg \langle\hat{a}^\dagger\hat{a}\rangle$, Eq. (1) simplifies to

$$I(\phi)\approx|c|^2+|c|\langle\hat{a}e^{i\phi}+\hat{a}^\dagger e^{-i\phi}\rangle. \tag{2}$$

Thus by changing the phase of the local oscillator ϕ one can measure the spectral decompositions of all quadratures,

$$\hat{X}_\phi=\hat{x}\cos\phi+\hat{p}\sin\phi, \tag{3}$$

$\hat{x}=(\hat{a}+\hat{a}^\dagger)/2$ and $\hat{p}=(\hat{a}-\hat{a}^\dagger)/(2i)$ being the canonically conjugated position and momentum operators. Such a set of measurements can be inverted to give the quantum state of the measured mode of light at the frequency ω. For a nice review of this technique see [7].

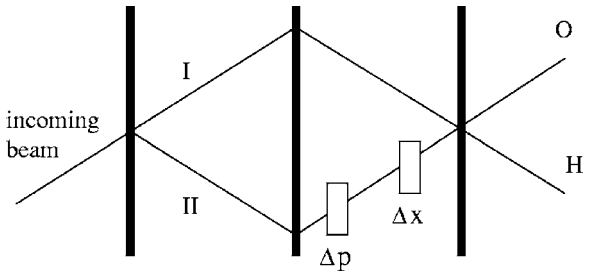

FIG. 1. Scheme of a perfect crystal neutron interferometer. The incoming beam is split at the first crystal plate, reflected at the middle plate, and recombined again at the third plate. The detector is placed in beam O where the visibility is higher due to the same number of reflections/transmissions. In addition to a position shift Δx, routinely used in neutron experiments, a momentum kick Δp has been added in path II in order to make the interferometric measurement tomographically complete; see text.

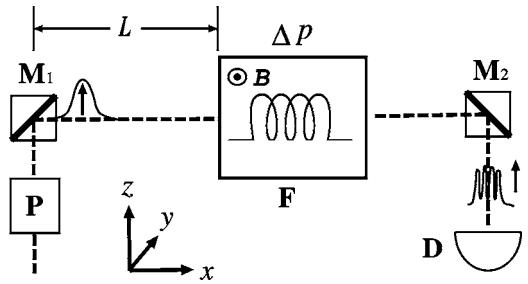

FIG. 2. Setup for the tomography of motional states of neutrons. M_1, M_2 are magnetic mirrors; L is the region of free propagation; B is the static homogeneous magnetic field controlling the momentum kick Δp; F is the box containing the static magnetic field (aligned along $-y$) and a rf coil; D is the detector; the state is "prepared" by P, which can be a chopper or a monochromator. The arrows denote the polarization of neutrons after reflections from the magnetic mirrors.

Unfortunately, no such local oscillators exist for neutrons. However, notice that massive particles experience a transformation of the type (3) in the course of free evolution:

$$x(t) = x + (p/m)t, \tag{4}$$

where m is the mass. Thus a free evolution of the wave packet, followed by a position sensitive measurement, yields information about a subset of quadratures X_ϕ, $\phi \in [0, \pi/2]$. Free evolution was utilized, e.g., for the reconstruction of the transversal motional states of helium atoms in Ref. [8]. Here we are interested in the *longitudinal* degrees of freedom. Since neutron detectors have very bad time resolution, the free evolution alone cannot be used to generate a tomographically complete set of measurements.

Feasible measurements on thermal neutrons consist of measurements of the contrast and phase of the interference fringes in an interferometric setup [see Fig. 1 (without momentum kick Δp)], and also a spectral analysis of the neutron beam using an adjustable Bragg-reflecting crystal plate together with a position sensitive detector. This set of observables is not tomographically complete because the measurable (complex) contrast of the interference pattern [6] ($\hbar = 1$),

$$\Gamma(\Delta x) = \langle \psi | e^{i\Delta x \hat{p}} | \psi \rangle = \int |a(p)|^2 e^{i\Delta x p} dp, \tag{5}$$

is not sensitive to the phase of the wave function in the momentum representation $a(p) = \langle p | \psi \rangle$, and no information about quadratures other than p is available.

Obviously, the situation would be different if one could shift both the position (phase) and the momentum of the incoming wave packet inside the interferometer. Such a thought experiment is shown in Fig. 1. In that case the measured contrast

$$\Gamma(\Delta p, \Delta x) = \mathrm{tr}\{\rho e^{i\Delta p \hat{x}} e^{i\Delta x \hat{p}}\} = \int e^{i(\Delta p)x} \langle x + \Delta x | \rho | x \rangle dx, \tag{6}$$

where ρ is the state to be reconstructed, would be related to the Wigner function describing the ensemble of measured neutrons

$$W(x,p) = \int \frac{dv}{2\pi} e^{-ivp} \langle x + v/2 | \rho | x - v/2 \rangle \tag{7}$$

by a simple integral transformation,

$$W(x,p) = \int \int \frac{du\, dv}{(2\pi)^2} e^{iuv/2 - iux - ivp} \Gamma(u,v). \tag{8}$$

Although this gedanken experiment looks simple, its experimental realization, according to Fig. 1, would be rather difficult. Large momentum kicks acquired by the neutron in the lower arm would change its de Broglie wavelength and spoil the Bragg reflection at the last crystal plate. Therefore we will now propose a modified scheme that can substitute the interferometric setup of Fig. 1.

III. SETUP

In the scheme shown in Fig. 2, the incoming neutrons polarized in the $+z$ direction are described by the state

$$|\Psi\rangle = |\psi\rangle |z_+\rangle, \tag{9}$$

where ψ denotes the spatial degrees of freedom. Initially, neutrons freely propagate through a distance L, undergoing a unitary transformation

$$U_1 = \exp[-i\hat{p}^2 L/(2p_0)]. \tag{10}$$

In the following, we will assume that the input wave packets have spread σ_p, central momentum p_0 and are quasimonochromatic, $\sigma_p/p_0 \simeq$ a few percent, so that in Eq. (10) $L = p_0 t/m$. This condition guarantees that the action of the rf coil (see below) is practically equivalent to a momentum "kick." The generalization to more general states will be presented elsewhere. After the region of free propagation, the

neutrons are let through a rf coil [9] placed in a static homogeneous magnetic field polarized along the $-y$ direction (see Fig. 2). Let us first discuss the action of the static magnetic field without the rf coil. Upon entering the interaction region the y_+ (y_-) spin component (both components corresponding to nondegenerate eigenstates of the system), is decelerated (accelerated). Upon leaving the interaction region the situation is reversed and the y_+ (y_-) spin component is accelerated (decelerated), so that the original momentum is restored. The only resulting net change is the introduction of a delay between the wave packet associated with the y_+ and y_- spin components. Inserting now into the static magnetic field a rf coil tuned to the transition energy between the y_+ and y_- eigenstates, the neutrons can now exchange rf photons with the coil while making a complete spin flip. As discussed above, upon entering the interaction region, the y_+ component is decelerated, then by exchanging a photon with the coil it flips and becomes a y_- component. Finally, having become a y_- component, it is decelerated for a second time when it exits the region where the static magnetic field is present. For the incoming y_- component the situation is reversed and we are left, after the neutron leaves the interaction region, with a net momentum difference Δp between the two wave packets associated with the different spin components. Hence, as a result of the interaction between the neutron and the magnetic fields, the y_+ component of the input state will be decelerated with respect to the y_- component. The momentum change Δp is controlled by the strength of the static field B and does not depend on the length of the interaction region. However, this length must be chosen in such a way that the flip between the y_+ and y_- spin projections will happen with 100% probability. Since the length of the coil is of the order of a few centimeters, the dispersion of the wave packet of the neutron in the coil can be neglected, and in the quasimonochromatic approximation the net momentum transfer can be described by the effective unitary operator

$$U_2 = e^{-i\Delta p\hat{x}/2}|y_-\rangle\langle y_+| + e^{i\Delta p\hat{x}/2}|y_+\rangle\langle y_-|, \tag{11}$$

where

$$\Delta p = \frac{2\mu Bm}{p_0}. \tag{12}$$

Prior to detection, the neutron spins are projected along the $+z$ direction again, so as to erase the which-way information stored in the polarization degree of freedom. The probability of a neutron being detected is given by the norm of the transmitted component,

$$P(\Delta x, \Delta p) = \mathrm{Tr}\{\Pi(\Delta p, \Delta x)\rho\}, \tag{13}$$

where ρ refers only to the spatial degrees of freedom and

$$\begin{aligned}\Pi(\Delta p, \Delta x) &= \langle z_+|U_1^\dagger U_2^\dagger|z_+\rangle\langle z_+|U_2U_1|z_+\rangle \\ &= (1 + e^{i(L/2p_0)\hat{p}^2}e^{i\Delta p\hat{x}}e^{-i(L/2p_0)\hat{p}^2})/4 + \text{H.c.} \\ &= (1 + e^{i\Delta p(\hat{x}+L\hat{p}/p_0)})/4 + \text{H.c.} \end{aligned} \tag{14}$$

$$= (1 + e^{i\Delta x\hat{p}}e^{i\Delta p\hat{x}}e^{-i\Delta x\Delta p/2})/4 + \text{H.c.}, \tag{15}$$

where we denoted

$$\Delta x = \frac{\Delta pL}{p_0} = \frac{2\mu BmL}{p_0^2}. \tag{16}$$

We stress that the operators in Eqs. (14) and (15) constitute positive-operator-valued measurements (POVM).

IV. DIRECT INVERSION

By comparing (15) with (6) one can easily see that the detection probability (13) reads

$$P(\Delta p, \Delta x) = \frac{1}{2} + \frac{1}{2}\,\mathrm{Re}\{\Gamma(\Delta p, \Delta x)e^{i\Delta x\Delta p/2}\}. \tag{17}$$

Since the beam is quasimonochromatic, $\sigma_p \ll p_0$ (say, by one or two orders of magnitude), one has for $\delta x = \pi/2p_0$,

$$\Gamma(\Delta p, \Delta x + \delta x) \simeq \Gamma(\Delta p, \Delta x)e^{i\pi/2} \tag{18}$$

from which the imaginary part of the complex degree of coherence $\Gamma(\Delta p, \Delta x)$ can be obtained.

Summarizing, the tomography of a neutron state consists in the following four steps.

(i) A set of pairs of independent variables $\{B_j, L_j\}$ is chosen covering a certain range $B \in [0, B_{\max}]$ and $L \in [0, L_{\max}]$.

(ii) For each pair B_j, L_j the shifts Δp_j in Eq. (12) and Δx_j in Eq. (16) are calculated, and the corresponding intensities $P(\Delta p_j, \Delta x_j)$ are measured with and without an auxiliary shift $\delta x = \pi/2$.

(iii) The complex degree of coherence $\Gamma(\Delta p_j, \Delta x_j)$ is calculated from the two intensities using Eqs. (17) and (18).

(iv) Finally, the Wigner function of the input neutrons is calculated with the help of the inversion formula (8), where the integrals are approximated by sums over Δx_j and Δp_j.

According to (8), the contrast $\Gamma(\Delta p, \Delta x)$ is essentially the Fourier transform of the Wigner function $W(x,p)$. Therefore the largest values of Δp and Δx are related to the smallest resolved details in x and p respectively. Namely (reinserting $\hbar$),

$$\Delta p_{\max} = \hbar/\delta x_{\min}, \quad \Delta x_{\mathrm{MAX}} = \hbar/\delta p_{\min}, \tag{19}$$

where $\delta x_{\min}$ and $\delta p_{\min}$ denote the x and p resolutions. By Eqs. (12) and (16) one gets

$$\delta x_{\min} = \frac{\hbar}{2\mu m}\frac{p_0}{B_{\max}}, \quad \delta p_{\min} = \frac{p_0}{L}\delta x_{\min}. \tag{20}$$

For a neutron of wavelength $\lambda_0 = 0.37$ nm [10], assuming the reasonable values $L_{\max} = 1$ m and $B_{\max} = 0.1$ T one gets $\delta x_{\min} = 60$ μm and $\delta p_{\min} = \hbar \times 10^6$ m^{-1}.

V. RADON INVERSION

It is interesting to give an alternative interpretation of the measurement proposed in Fig. 2. Notice that the POVM elements in Eq. (14) can also be restated in terms of quadrature operators,

$$\Pi(\Delta p,\Delta x) = (1/4)(1 + e^{i\omega\hat{X}_\theta}) + \text{H.c.}, \tag{21}$$

where (in fixed units)

$$\hat{X}_\theta = \hat{x}\cos\theta + \hat{p}\sin\theta, \quad \tan\theta = \frac{\Delta x}{\Delta p} = \frac{L}{p_0}, \tag{22}$$

and $\omega = \sqrt{\Delta x^2 + \Delta p^2}$. Thus, for a fixed θ, the data contain information about the characteristic function of the quadrature $\hat{X}_\theta$,

$$P(\Delta p,\Delta x) = 1/2 + \text{Re}\{C_{X_\theta}(\omega)\}/2, \tag{23}$$

$$\langle C_{X_\theta}(\omega)\rangle = \int P_{X_\theta}(x)e^{i\omega x}dx, \tag{24}$$

where $P_{X_\theta}(x) = \text{tr}\{\rho\delta(X_\theta - x)\}$ is the probability density of the quadrature X_θ. By changing L one changes the measured quadrature, while ω, which depends on both L and B, determines the observed spatial frequency of the probability distribution of this quadrature. The observed quadratures range from $\hat{x}$ (for $L=0$) to $\hat{p}$ (for $L\to\infty$). From the measurement of $C_{X_\theta}(\omega)$, the "shadows" $P_{X_\theta}(x)$ of the Wigner function can be obtained by a Fourier transformation, which in turn yields the Wigner function by an inverse Radon transformation. This is an alternative way to reconstruct the Wigner function from the measured data in the setup of Fig. 2.

VI. STATISTICAL INVERSION

The procedures outlined above, based on the direct inversion formula (8), have several drawbacks. (i) Realistic data are always noisy. In that case, formula (8) can yield unphysical results, such as the Wigner representation of a nonpositive definite operator. (ii) The Wigner function in Eq. (8) depends on the measured data indirectly, through the complex degree of coherence Γ, which itself has to be estimated with the help of an auxiliary position shifter. This intermediate step is, certainly, not necessary as all available information about the Wigner function of the incoming neutrons is contained in the raw measured data, without any auxiliary position shift. In order to avoid these problems, we propose to use the maximum-likelihood quantum state reconstruction [5,11,12]. The main advantages of this method compared to the above direct inversion are as follows. (i) Asymptotically, for large data samples it provides the best performance available. (ii) Any prior information about the measured neutrons and the known statistics of the experiment can be used to increase the accuracy of the reconstruction. (iii) The existing physical constraints can be easily incorporated into the reconstruction. Most notably, this technique guarantees the positivity of the reconstructed density operator. (iv) It can be directly applied to raw counted data.

Let us briefly illustrate this method. For simplicity, in the following we will replace pairs of position and momentum shifts Δx and Δp by a single subscript j, $\{\Delta x,\Delta p\}\to j$. This subscript will denote all combinations of Δx and Δp used in the experiment.

The counted statistics of thermal neutrons is known to be Poissonian; see, e.g., [13]. Consequently the likelihood function to be maximized has the Poissonian form,

$$L(\rho,I_0) = \prod_j \frac{(I_0P_j)^{n_j}}{n_j!}e^{-I_0P_j}, \tag{25}$$

where I_0 is the intensity of the incoming neutron beam and n_j is the number of neutrons counted for the corresponding setting j of position and momentum shifts. Maximizing L is the same as maximizing its logarithm,

$$\ln L(\rho,I_0) = \sum_j n_j \ln(I_0P_j) - I_0\sum_j P_j - \sum_j \ln(n_j!). \tag{26}$$

To be consistent, we will estimate the intensity I_0 together with the neutron state ρ. Setting the derivative of $\ln L$ with respect to the intensity equal to zero, we get

$$I_0 = \frac{\sum_j n_j}{\sum_j P_j}. \tag{27}$$

Substituting this value back into Eq. (26) and keeping only state-dependent terms, we obtain a modified log-likelihood

$$\ln L(\rho) = \sum_j n_j \frac{P_j(\rho)}{\sum_{j'} P_{j'}(\rho)}, \tag{28}$$

which can also be interpreted as the relative entropy of the measured data n_j with respect to the (renormalized) theoretical probabilities $P_j/\Sigma P_j$. This functional should now be maximized with respect to the unknown state ρ. As has been shown in [11,12], the maximum-likely density matrix can be obtained as a fixed point of the iterations of a nonlinear operator map,

$$\sum_j \frac{n_j}{P_j(\rho)}\Pi_j\rho = \frac{\sum_{j'} n_{j'}}{\sum_{j'} P_{j'}(\rho)}\sum_j \Pi_j\rho, \tag{29}$$

where Π_j are the POVM elements in Eq. (15).

VII. SIMULATION

As follows from the parameter estimates given after Eq. (20), the proposed tomographic scheme using thermal neutrons will likely have sufficient resolution in momentum. On the other hand, even for well monochromatized thermal beams, the resolution in position is expected to be worse (possibly even by several orders of magnitude) than the typical coherence lengths. The simulations in Fig. 3 illustrate the effect of the restricted range of Δp on the reconstruction. Consider first the reconstruction of a minimum uncertainty Gaussian wave packet in its moving frame, parametrized by its coherence length l_{coh},

$$|\Psi_G\rangle \propto \int \exp(-k^2l_{\text{coh}}^2)|k\rangle dk. \tag{30}$$

(The choice of a minimum uncertainty state is only for illustrative purposes.) Provided the apparatus has a sufficient spa-

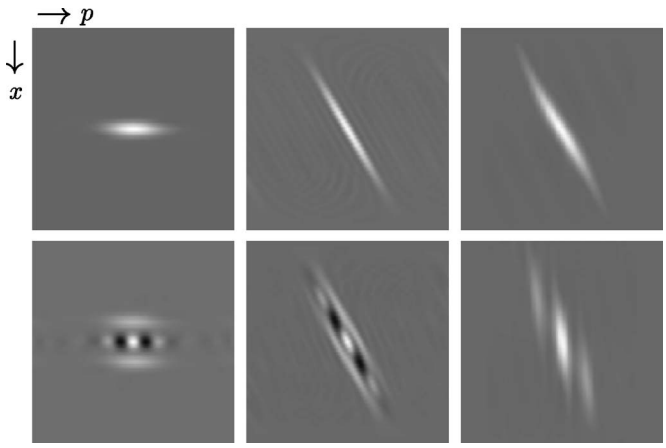

FIG. 3. Reconstructed Wigner functions of Gaussian states (upper row) and superpositions of Gaussian states ("cat states;" lower row) from the simulated data. A 50×50 matrix of Δx and Δp shifts was used for the maximum-likelihood inversion, based on Eq. (29). Left column, reconstructed original states; middle column, reconstructed time-evolved states with a resolution $\delta x_{\min}/l_{\mathrm{coh}}=1/2$; right column, reconstructed time-evolved states with reduced resolution $\delta x_{\min}/l_{\mathrm{coh}}=10$. Gray is the zero level; white (black) represents positive (negative) values.

tial resolution $\delta x_{\min}<l_{\mathrm{coh}}$, a faithful reconstruction is readily obtained, see the upper left panel. More realistic measurement with $\delta x_{\min}>l_{\mathrm{coh}}$ would obviously yield a Wigner function smoothed out along the x axis. However, the states measured in a real experiment are not going to be minimum uncertainty states. The experimenter will rather deal with time-evolved states

$$|\Psi(T)\rangle \propto \int \exp(ik^2T/2m - k^2l_{\mathrm{coh}}^2)|k\rangle dk \tag{31}$$

that are strongly affected by dispersion. As a consequence, the wave packet spread very soon becomes larger than the resolution limit,

$$\delta x_T \sim T/(ml_{\mathrm{coh}}) \gg \delta x_{\min}, \tag{32}$$

and a good reconstruction can be achieved with a realistic apparatus. Compare the upper middle and right panels, showing reconstructions with a sufficient resolution $\delta x_{\min}=l_{\mathrm{coh}}/2$ and a reduced (but more realistic) resolution $\delta x_{\min}=10l_{\mathrm{coh}}$.

The imaging of nonclassical states is a much more delicate problem. Let us consider the superposition of spatially separated Gaussian states (Schrödinger cat states),

$$|\Psi_{\mathrm{cat}}\rangle \propto [1+\exp(i\hat{p}\Delta)]|\Psi_G\rangle. \tag{33}$$

Such states can be prepared, e.g., by means of a double-loop perfect crystal interferometer [14]. As has been shown in Ref. [10], by splitting an incoming neutron Gaussian wave packet at the input plate of a perfect-crystal neutron interferometer, delaying one component with respect to the other using a sufficiently large phase shifter Δ, and recombining them again at the output crystal plate, the preparation of thermal neutron cat states is possible, with separations exceeding the corresponding coherence lengths of the individual components $\Delta\gg l_{\mathrm{coh}}$. Provided the apparatus has sufficient resolution, the nonclassicality of this state is manifested by the negative regions of the reconstructed Wigner function, see the lower left panel of Fig. 3. Taking dispersion into account, the ordering of the relevant parameters is $l_{\mathrm{coh}}<\Delta<\delta x_T$, and one can easily obtain $\delta x_{\min}<\delta x_T$. As the simulations show, a realistic measurement, whose position resolution is much worse than the coherence lengths of the individual cat state components, tends to wipe out the negative regions of the reconstructed Wigner function; compare the lower middle and right panels of Fig. 3. On the other hand, the main features of such exotic states, such as their non-Gaussian character and also the global spatial properties of which little is known today, should still be accessible to a realistic wave packet tomography. To resolve more subtle quantum interference effects of the order of the coherence length, more refined experimental techniques may, however, be needed. An idea could be to replace thermal neutrons by ultracold neutrons, for which much larger momentum shifts Δp (and thus much smaller $\delta x_{\min}$, possibly even smaller than Δ) can be obtained.

VIII. CONCLUSION

We have proposed and analyzed an experimental scheme for determining the motional states of neutrons. With the help of a magnetic field and free propagation, the apparatus proposed in this paper realizes quadrature measurements on neutrons by measuring the overlaps of the two transformed components of the initial state. This is an analog of the quantum optical homodyne detection in neutron optics, achieved without the use of a strong coherent source of neutrons.

ACKNOWLEDGMENTS

J.Ř. and S.P. are grateful for the kind hospitality at the Physics Department of the University of Bari and the Department of Optics of Palacký University, respectively. This work was partially supported by the Bilateral Research Program between Italy and the Czech Republic PH1 on "Decoherence and Quantum Measurements" and by the Research Project No. MSM 6198959213 of the Czech Ministry of Education. T.Y. would like to thank the Japanese Ministry of Education for financial support.

[1] S. Weigert, Phys. Rev. A **45**, 7688 (1992).
[2] S. Weigert, Phys. Rev. A **53**, 2078 (1996).
[3] K. Vogel and H. Risken, Phys. Rev. A **40**, R2847 (1989).
[4] D. T. Smithey, M. Beck, M. G. Raymer, and A. Faridani, Phys. Rev. Lett. **70**, 1244 (1993).
[5] *Quantum State Estimation*, M. Paris and J. Řeháček, edited by Lecture Notes in Physics Vol. 649 (Springer, Berlin, 2004).
[6] H. Rauch and S. A. Werner, *Neutron Interferometry* (Oxford University Press, Oxford, 2000).
[7] M. Raymer and M. Beck, in *Quantum State Estimation*, edited by M. Paris and J. Řeháček, Lecture Notes in Physics Vol. 649 (Springer, Berlin, 2004).
[8] C. Kurtsiefer, T. Pfau, and J. Mlynek, Nature (London) **386**, 150 (1997).
[9] G. Badurek, H. Rauch, and A. Zeilinger, Z. Phys. B: Condens. Matter **38**, 303 (1980).
[10] G. Badurek, H. Rauch, M. Suda, and H. Weinfurter, Opt. Commun. **179**, 13 (2000).
[11] Z. Hradil, Phys. Rev. A **55**, R1561 (1997).
[12] J. Řeháček, Z. Hradil, and M. Ježek, Phys. Rev. A **63**, 040303(R) (2001).
[13] H. Rauch, J. Summhammer, M. Zawisky, and E. Jericha, Phys. Rev. A **42**, 3726 (1990).
[14] M. Baron, H. Rauch, and M. Suda, J. Opt. B: Quantum Semiclassical Opt. **5**, S241 (2003).